



Contents lists available at ScienceDirect

Biochimica et Biophysica Acta

journal homepage: www.elsevier.com/locate/bbamem

Interactions of antimicrobial peptide from C-terminus of myotoxin II with phospholipid mono- and bilayers

Amy Won, Anatoli Ianoul*

Department of Chemistry, Carleton University, 1125 Colonel By Dr. Ottawa ON Canada

ARTICLE INFO

Article history:

Received 8 June 2009

Received in revised form 10 July 2009

Accepted 17 July 2009

Available online xxxx

Keywords:

Antimicrobial peptide

Phospholipid

Monolayer

Atomic force microscopy

Model cell membrane

ABSTRACT

Comparative studies of the effect of a short synthetic cationic peptide, pEM-2 (KKWRWWLKALAKK), derived from the C-terminus of myotoxin II from the venom of the snake *Bothrops asper* on phospholipid mono- and bilayers were performed by means of Langmuir Blodgett (LB) monolayer technique, atomic force microscopy and calcein leakage assay. Phospholipid mono- and bilayers composed of single zwitterionic or anionic phospholipids as well as lipid mixtures mimicking bacterial cell membrane were used. LB measurements indicate that the peptide binds to both anionic and zwitterionic phospholipid monolayers at low surface pressure but only to anionic at high surface pressure. Preferential interaction of the peptide with anionic phospholipid monolayer is also supported by a more pronounced change of the monolayer pressure/area isotherms induced by the peptide. AFM imaging reveals the presence of nanoscale aggregates in lipid/peptide mixture monolayers. At the same time, calcein leakage experiment demonstrated that pEM-2 induces stronger disruption of zwitterionic than anionic bilayers. Results of the study indicate that electrostatic interactions play a significant role in the initial recognition and binding of pEM-2 to the cell membrane. However, membrane rupturing activity of the peptide depends on interactions other than simple ionic attraction.

© 2009 Elsevier B.V. All rights reserved.

1. Introduction

Antimicrobial peptides (AMP) are components of the innate defence system of many organisms and display potent antimicrobial activity against a variety of microorganisms by direct action (disrupting bacterial cell membrane) or by modulating an immune system response [1–6]. AMP are often alpha helical, composed of 9 to 100 amino acids with a combined molecular weight of 10 kDa or less, contain an excess positive charge of +2 to +9 arising from mainly lysine and arginine, and are composed of around 50% hydrophobic residues [1,7,8].

Although some AMP have been found to interact with intracellular targets, it is believed that interactions between the peptides and the cell membrane play an essential role in their mode of action [9]. The outer leaflet of the Gram-negative bacteria contains lipopolysaccharide (LPS) and the single membrane of Gram-positive bacteria contains acidic polysaccharides [1–6] giving a net negative charge to the bacterial membrane surface. Moreover, inner leaflets of Gram-negative and Gram-positive bacteria are predominantly composed of negatively charged phosphatidyl glycerol (PG) and phosphatidyl ethanolamine (PE). Mammalian cells, on the other hand, contain predominantly zwitterionic phosphatidylcholine (PC), cholesterol

and sphingomyelin in the outer leaflet and negatively charged phosphatidylserine (PS) in the inner leaflet [10]. Due to electrostatic interactions, positively charged AMP preferentially target negatively charged cell membranes of bacteria.

Despite the fact that natural AMP have been studied for a considerable period of time, only four peptides have advanced into phase 3 clinical trials, but none have been approved for medical use. This is mainly due to the relatively high toxicity and rapid in vivo degradation which significantly reduces their bioavailability [1–6]. Thus a number of synthetic AMP have been studied and derived to circumvent the proteolytic susceptibility [1,11]. A series of 10 synthetic peptides was derived from the C-terminus of myotoxin II of *Bothrops asper* (KKYRYLKLCKK) which is homologous to catalytically inactive Lys 49 phospholipase A₂ [12–14]. In this series peptides were obtained by substituting one or several tyrosine residues with tryptophan. A general correlation between the number of tryptophan substitutions and microbicidal potency was observed. However, together with high bactericidal activity most of these newly derived peptides were more cytolytic towards skeletal muscle cells, thus limiting their potential application in vivo [13]. One of the derivatives called pEM-2 was obtained through substituting 117, 119 and 120 Tyr with Trp, and 123 Pro and 125 Cys with Ala giving the sequence KKWRWWLKALAKK. This derivative was found to maintain high bactericidal [12,13], fungicidal [15] and also antitumor activities [16] while having reduced toxicity towards eukaryotic cells. The all-D enantiomer of pEM-2 retains the same bactericidal potency as the

* Corresponding author. Tel.: +1 613 520 26006043; fax: +1 613 520 3749.
E-mail address: anatoli_ianoul@carleton.ca (A. Ianoul).

L-enantiomer but is also less susceptible to degradation by proteases [12] suggesting a non specific nature of interactions between the peptide and the target. In this work the role of hydrophobic and ionic components in these non specific interactions was explored by Langmuir Blodgett (LB) technique, atomic force microscopy (AFM) as well as calcein leakage assay.

2. Experimental

2.1. Chemicals

1,2-Dipalmitoyl-*sn*-Glycero-3-Phosphocholine (DPPC), 1,2-Dipalmitoyl-*sn*-Glycero-3-[Phospho-*rac*-(1-glycerol)] (DPPG), 1,2-Dioleoyl-*sn*-Glycero-3-Phosphoethanolamine (DOPE), 1,2-Dioleoyl-*sn*-Glycero-3-Phospho-(1'-*rac*-glycerol) (sodium salt) (DOPG), 1,1',2,2'-tetramyristoyl cardiolipin (sodium salt) (CL), and *E. coli* extract were purchased from Avanti Polar Lipids Inc. 1 mg/ml solutions of the lipids were prepared in chloroform (spectroscopy grade, Caledon)/ethanol (Branton) (3:1, v/v) mixture. Antimicrobial peptide pEM-2 was synthesized by Gen Script Corporation (>98% purity, with unmodified amino and carboxyl ends). Stock solution of the peptide (76.68 μ M) was prepared in phosphate buffer saline (PBS, 0.01 M, 138 mM NaCl, and 2.7 mM KCl) pH 7.4 (Sigma).

3. Methods

Monolayers were prepared on a Langmuir Blodgett (LB) trough (NIMA 311-D, Coventry, U.K.) using PBS (~200 ml) as the subphase. Monolayers of pEM-2 were prepared by adding appropriate amount of the peptide stock solution to the subphase to obtain the final peptide trough concentrations between 100 and 842 nM. The trough was allowed to equilibrate for 25 min and at least 5 compression–expansion isotherm cycles were performed before the final surface pressure/area isotherm was recorded with a barrier speed of 5 or 20 cm^2/min . After that the monolayer was transferred to a freshly cleaved, hydrophilic $2.5 \times 2.5 \text{ cm}^2$ mica sheet by vertical deposition with a dipping speed of 2 mm/min at the surface pressure of between 7 and 15 mN/m. Transfer ratios of 85–100% were typical.

Phospholipid monolayers were prepared by spreading 30 μ l of the 1 mg/ml lipid stock solution at the interface. After the solvent evaporation (15 min), the monolayer was annealed by performing at least two compression/expansion cycles.

For the incorporation kinetic experiments, the lipid monolayers were compressed to 7.5 and 30 mN/m pressure, and the peptide was injected under the monolayer. Increase of the monolayer surface area with time at constant surface pressure was recorded.

For the lipid/peptide mixture experiments the lipid monolayers were expanded and the appropriate amount of the peptide was injected into the subphase under the lipid monolayer. The system was allowed to equilibrate for 20–30 min to provide uniform pEM-2 distribution in the trough. The pressure/area isotherm of the lipid/peptide monolayer was recorded and the monolayer was transferred to a mica sheet for further AFM analysis.

3.1. Calcein leakage assay

For this assay six different model cell membranes were used: pure DPPC, pure DPPG, *Escherichia coli* model (DOPE/DOPG 80/20 mol%), *Staphylococcus aureus* model (DOPG/CL 55/45 mol%) and *Bacillus subtilis* model (DOPE/DOPG/CL 12/84/4 mol%) [17].

Small unilamellar vesicles were prepared by dissolving the appropriate amount of lipid in chloroform, drying the solvent under a stream of nitrogen and keeping the sample under vacuum for at least 24 h to ensure complete solvent removal. The obtained lipid films were hydrated in leakage buffer (10 mM Tris–HCl (Bioshop), 150 mM NaCl, 1 mM EDTA (Bioshop) pH 7.45 in 18.2 M Ω MilliQ water)

containing 70 mM calcein (Fluorescein-bis(methyliminodiacetic acid), Sigma) to obtain the final lipid concentration of 1 mg/ml. Lipid suspensions were sonicated with Misonix ultrasonicator for 2.5 h. Five freeze/thaw cycles were performed to maximize calcein encapsulation. Free calcein was separated from encapsulated calcein with a Sephadex G-50 size exclusion column using leakage buffer for equilibrium and elution (10 ml).

Leakage experiments were carried out using 2 ml of calcein-containing vesicles diluted 20 times with the leakage buffer on a Varian Cary Eclipse spectrofluorimeter. Measurements were carried out with excitation and emission wavelength determined for each experiment (475 nm to 490 nm and 510 nm to 525 nm, respectively). Excitation and emission slits were 2.5 nm, photomultiplier tube voltage was 540 V, and integration time was 1.0 s. The baseline fluorescence (F_0) was monitored before the addition of the peptide for 30 s. After the peptide was added the fluorescence signal intensity was monitored for approximately 15 min or until no further changes occurred. The final fluorescence intensity signal F was then measured. To determine the maximum fluorescence signal corresponding to complete disruption of the vesicles (F_M), 100 μ l of 10% triton X-100 (Bioshop) was added to the mixture at the end of the experiment and fluorescence intensity increase was monitored for 5 min. The leakage fraction was calculated as: %leakage = $[(F - F_0) \times 100\%] / (F_M - F_0)$.

The concentration of lipid phosphorus was measured by phosphate assay [18]. Vesicles with calcein (500 μ l) were mixed with 0.1 ml of KNO_3 and heated with a Bunsen burner to form potassium pyrophosphate on flame. After the addition of 0.3 ml of 1 M HCl and boiling in a water bath for 15 min, potassium pyrophosphate was hydrolyzed back into phosphate. Then 4.6 ml of 0.22% ammonium molybdate (Bioshop) and 0.2 ml Fiske–Subbarow reducing agent were added followed by vigorous stirring. The solution was incubating in a water bath at 40°C for 15 min. Absorption of the signal at 835 nm was measured. Fiske–Subbarow reagent was prepared by mixing 40 ml of 15% (w/v) sodium bisulfate (Acros Organic), 0.2 g sodium sulfite (Bioshop) and 0.1 g of 1-amino-4-naphtholsulfonic acid (Ricca Chemical Company). The solution was filtered and stored in the dark at 4 °C. The phosphate standard solutions were prepared using sodium phosphate monobasic up to 1 mM in 18.2 M Ω MilliQ water.

3.2. AFM imaging

The topography images of the monolayers were obtained with an Ntegra (NTMDT, Russia) atomic force microscope in semi contact mode in air at 23 °C with 512×512 points per image. A $100 \times 100 \mu\text{m}^2$ scanner (Ntegra) and cantilevers with rotated monolithic silicon tips (125 μm -long, 40 N/m spring constant Tap 300Al, resonance frequency 315 kHz, Budget Sensors) were used for all topographic measurements. The typical scan rate was 0.5 Hz.

4. Results and discussion

4.1. Monolayers of pEM-2

Monolayers of pEM-2 at the air–water interface were obtained by injecting the peptide into the subphase and allowing the system to equilibrate. At equilibrium a fraction of the peptide adsorbs at the interface and forms a monolayer. Fig. 1A shows LB isotherms obtained for pEM-2 at peptide concentrations up to 842 nM, which is comparable to minimum microbicidal concentration (MMC) against a number of bacteria, including *E. coli* and *S. aureus* [12]. The surface pressure increases almost linearly with decreasing surface area till approximately 15 mN/m. At approximately 15 mN/m the slope of the isotherm changes indicating that the peptide is lost to the subphase during the compression [19]. The expansion isotherms do not overlap with the compression isotherms signaling the loss of pEM-2 into the subphase above certain pressures. After the complete expansion of the

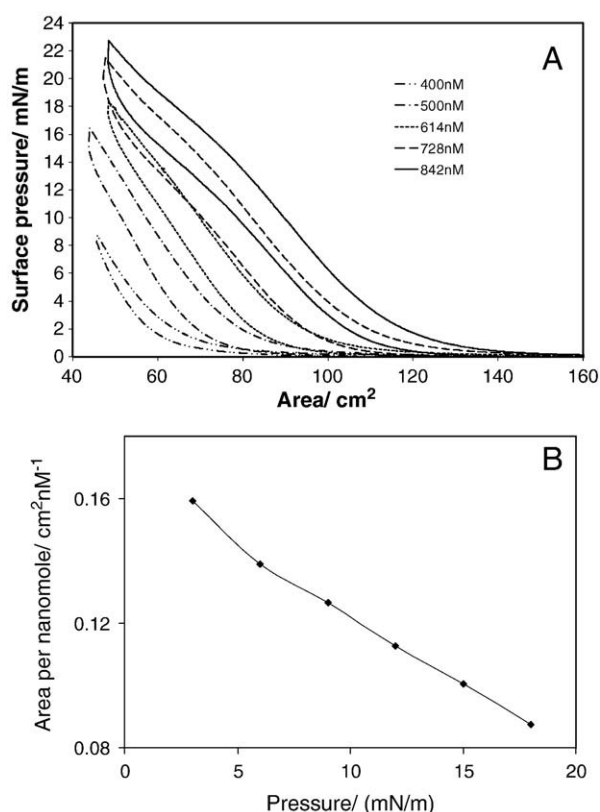


Fig. 1. (A) Langmuir-Blodgett compression–expansion isotherms for pEM-2 monolayer of different peptide concentrations: 400 nM; -.-.- 500 nM; ··· 614 nM; – 728 nM; — 800 nM. Compression and expansion isotherms are shown. Hysteresis observed suggests the loss of pEM-2 from the interface into the subphase during the compression. (B) Area per nanomole as a function of surface pressure. Average data calculated for different pEM-2 concentrations are presented.

monolayer, the peptide re-adsorbs back onto the interface. At higher peptide concentration in the trough, higher surface pressure can be achieved leading to increase in the hysteresis. Such behavior has been observed for other antimicrobial peptides [19].

In this monolayer experiment pEM-2 was added directly into the subphase rather than deposited at the interface. This method of introducing the peptide is more representative of the natural association phenomena of a peptide with a biological membrane [19–21]. At the same time, since the amount of the peptide at the interface is not known it is impossible to calculate the molecular area for pEM-2 in the monolayer. Instead, the increase in the monolayer surface area was related to the total peptide concentration in the trough. Fig. 1B shows the surface area occupied by pEM-2 relative to the peptide concentration as a function of the surface pressure. In the 4–15 mN/m surface pressure range the area slowly decreases from 0.16 to 0.08 cm²/nM. These values were calculated from the compression isotherms (Fig. 1A) and represent the upper limit for the area as the expansion isotherms would give significantly lower values due to the loss of the peptide into the subphase. However, these numbers provide some quantitative measure of the peptide surface activity.

The monolayers were transferred onto mica at 7 and 15 mN/m surface pressures for further AFM analysis. AFM measurements however did not reveal any aggregation of the peptide at the substrate (data not shown).

4.2. Kinetics of pEM-2 binding to lipid monolayer

Since most antimicrobial peptides exhibit their activity at the level of bacterial cell membrane [9], model cell membranes, such as

phospholipid monolayers at the air/water interface are often used in studies of AMP [19–25]. The effect of membrane lipid composition on binding properties of pEM-2 was studied by conducting insertion experiments with the peptide injected into the subphase under the monolayer of zwitterionic DPPC, anionic DPPG phospholipids or *E. coli* extract maintained at a constant surface pressure (7.5 or 30 mN/m). The peptide final concentration in the trough was 400 nM, which is comparable to MMC [12]. Time dependence of the area increase at constant surface pressure was measured (Fig. 2).

At 7.5 mN/m the peptide readily inserts into monolayers of all three lipid types with insertion half times around 1000 s (Fig. 2A). However the degree of the area change is different. For DPPC monolayer the relative area increase is 20% whereas for DPPG and for *E. coli* extract it is almost 35% giving relative molar area change $\Delta\sigma/(\sigma \times c)$ 4.8×10^{-4} nM⁻¹ for DPPC and 8×10^{-4} nM⁻¹ for DPPG, where σ is surface area, $\Delta\sigma$ is the area change and c is the peptide trough concentration.

The insertion experiment was also performed with the monolayers pre-compressed to 30 mN/m (Fig. 2B). After the peptide injection, the relative area change was found to be 2.5% for DPPG, ~1% for *E. coli* extract and barely any change was observed for DPPC. Relative molar area change $\Delta\sigma/(\sigma \times c)$ was found to be 5.4×10^{-5} nM⁻¹ for pEM-2 insertion into DPPG, 2.5×10^{-5} nM⁻¹ for insertion into *E. coli* extract and essentially zero (9.4×10^{-8} nM⁻¹) for insertion into DPPC. The insertion half time was ~500 s which is shorter than for the 7.5 mN/m experiment.

From this experiment it is clear that the nature of the head group plays an essential role in the initial pEM-2/membrane recognition and binding. At low surface pressure of 7.5 mN/m the peptide is capable of incorporating into both anionic and zwitterionic membranes because of the intrinsic surface activity of the peptide. However, at the

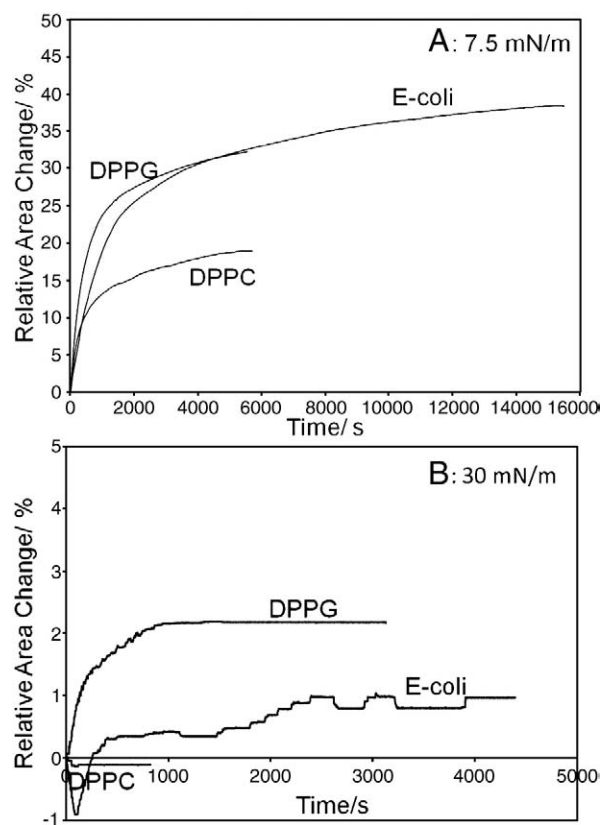


Fig. 2. Relative increase of the area of DPPG (30 μ l, 1 mg/ml), DPPC (30 μ l, 1 mg/ml) or *E. coli* (20 μ l, 1 mg/ml) monolayer compressed to 7.5 mN/m (A) or 30 mN/m (B) as a function of time after pEM-2 was injected into the subphase. Final pEM-2 concentration was 400 nM.

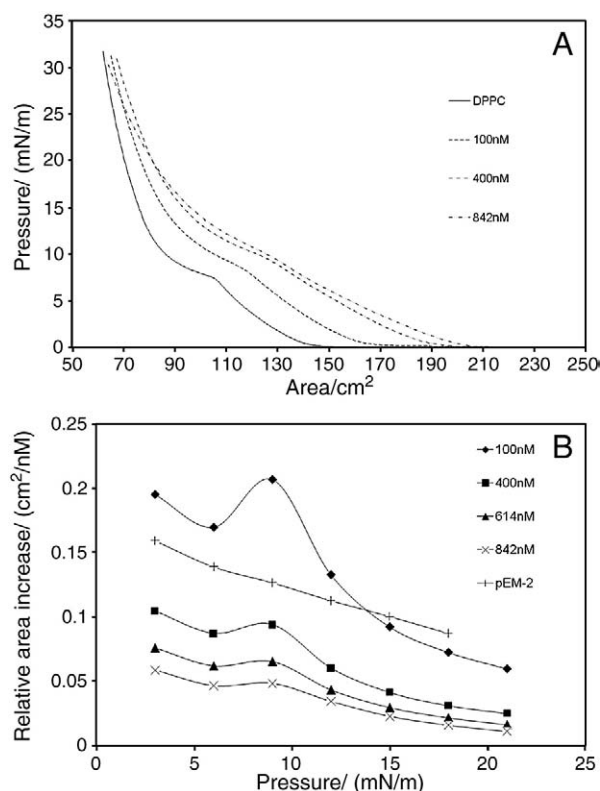


Fig. 3. (A) Effect of different pEM-2 concentrations on the compression isotherms of a 30 μ l 1 mg/ml DPPC monolayer. Peptide concentrations: — 0 nM; - - - 100 nM; ···· 400 nM; - · - · 842 nM. (B) Relative area increase at different pressures calculated from the isotherms shown in panel A. Indicated are final concentrations of pEM-2 in the trough. For comparison surface area of pEM-2 monolayer alone is shown (-+- pEM-2).

biologically relevant pressure of 30 mN/m and peptide concentration of 400 nM, pEM-2 has a much higher affinity to anionic DPPG membranes and some modest but detectable affinity to the *E. coli* membrane which also carries some negative charge. This is caused by the additional electrostatic attraction between the peptide and the anionic model cell membrane.

4.3. Interaction of pEM-2 with monolayer of zwitterionic phospholipid DPPC

LB isotherms for monolayers of zwitterionic phospholipid DPPC in the presence of pEM-2 were further obtained (Fig. 3A). In this set of experiments phospholipid monolayers were first prepared and the peptide was injected into the subphase with the monolayer fully expanded (0 mN/m surface pressure).

Compression isotherm for a monolayer of pure DPPC shows a characteristic liquid expanded–liquid condensed phase transition at 7.5 mN/m (Fig. 3A, solid line) [26]. When pEM-2 is added to the trough with DPPC monolayer fully expanded, the peptide tends to adsorb at the air/water interface. Upon further compression the resulting pEM-2/DPPC mixture monolayer occupies greater area than the pure DPPC monolayer. With increasing concentration of pEM-2 this total area increases as well (Fig. 3A). The phase transition around 7.5 mN/m is still present when the concentration of the peptide is as high as 842 nM. At higher surface pressure (26–31 mN/m), surface areas occupied by the monolayer of DPPC alone and pEM-2/DPPC mixtures are very similar; suggesting that at this pressure most of the peptide is lost into the subphase.

The changes in the surface area with respect to the peptide concentration were further calculated (Fig. 3B). Each curve represents a relative increase in the area of the monolayer (calculated as: area of the pEM-2/DPPC mixture minus the area of pure DPPC and divided by the total concentration of the peptide in the trough) for different final pEM-2 concentrations. For comparison, the Fig. 1B data for the peptide monolayer alone are presented as -+- . As can be seen from Fig. 3B, up to 100 nM the increase of surface area upon the peptide addition varies from 0.2 to 0.02 cm^2/nM (Fig. 3B, - \blacklozenge -) and is greater or comparable to the area occupied by the peptide alone (Fig. 3B, line -+-). Therefore, the peptide has slightly higher affinity to the monolayer of DPPC rather than the air/water interface, especially at the lower surface pressure.

Fig. 4 shows AFM topography images of pEM-2/DPPC monolayer deposited onto mica substrate at 30 mN/m for two pEM-2 concentrations: 100 nM and 842 nM. Some small aggregates can be observed in both cases. There are two kinds of aggregates observed at 100 nM with corresponding heights of 2 nm and 4–6 nm respectively and lateral dimensions of 30–50 nm. At 842 nM we can only detect aggregates with the average height of 3–4 nm and lateral size of 30–50 nm. In both cases the small clusters are organized into larger irregularly shaped micro-domains. The surface area occupied by the clusters is similar at both concentrations, which is consistent with LB data showing a very similar monolayer surface area at 30 mN/m for 100 nM and 842 nM (Fig. 3A). Since no aggregation was observed for the monolayers of the peptide alone, it is reasonable to assume that the observed clusters result from the peptide interaction with the lipid and the formation of some lipid/peptide aggregates. Similar behavior was recently observed for other AMP [23].

4.4. Interaction of pEM-2 with monolayer of anionic phospholipid DPPG

LB isotherms for monolayers of anionic phospholipid DPPG in the presence of pEM-2 were further obtained (Fig. 5A). Similar to the previous experiment phospholipid monolayers were first prepared

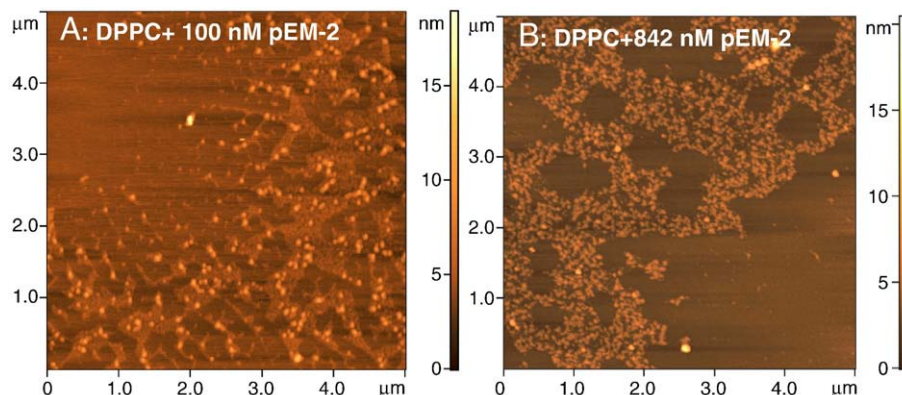


Fig. 4. AFM topography images of DPPC/pEM-2 monolayers transferred at 30 mN/m. pEM-2 subphase concentrations were 100 nM and 842 nM.

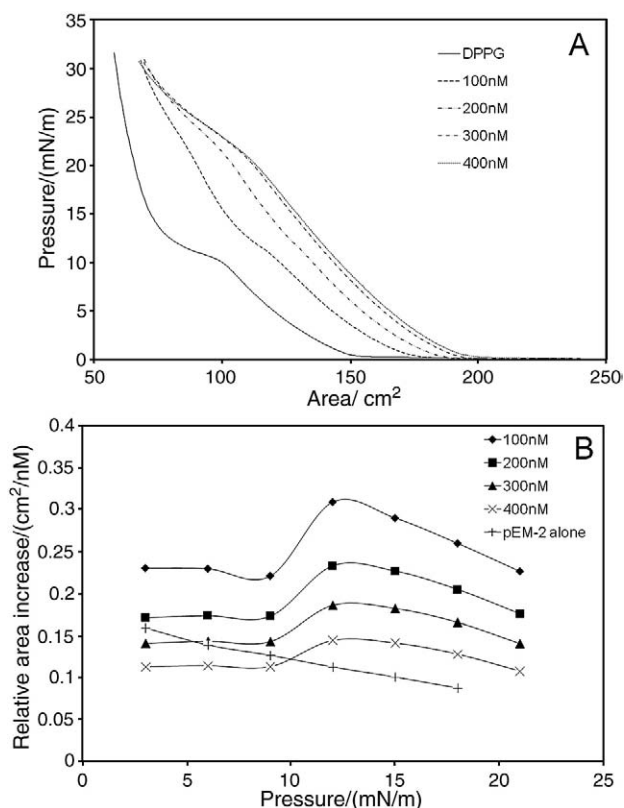


Fig. 5. (A) Effect of increasing pEM-2 concentration on the compression isotherms of a 30 μ l 1 mg/ml DPPG monolayer. Peptide concentrations: — 0 nM; - - - 100 nM; ····· 200 nM; - · - · 300 nM; and ····· 400 nM. (B) Relative area increase at different pressures calculated from panel A isotherms. Indicated are final concentrations of pEM-2 in the trough. For comparison surface area of pEM-2 monolayer alone is shown (-+- pEM-2).

and the peptide was injected into the subphase with the monolayer fully expanded (0 mN/m surface pressure).

The compression isotherms of DPPG alone and with increasing concentration of pEM-2 are presented in Fig. 5A. A characteristic phase transition can be observed at \sim 10 mN/m. DPPG has been previously shown to exhibit first-order phase transition upon monolayer compression and the pseudo-plateau region seen in the compression isotherm corresponds to the liquid expanded–liquid condensed transition [27–29].

With increasing pEM-2 concentration the phase transition around 10 mN/m disappears, the monolayer surface area increases, and a second transition at 20–25 mN/m appears. In the 100–400 nM concentration range, the relative increase in the surface area of the DPPG monolayer (Fig. 5B) was found to be between 0.1 and 0.3 cm²/nM, which is greater than for the DPPC containing monolayer (Fig. 3B) and in most cases is greater than the area occupied by pEM-2 alone (Fig. 5B, line -+-). At the same time, at a higher surface pressure of 30 mN/m, the pEM-2/DPPG monolayer surface area is almost independent of the peptide trough concentration but is considerably greater than for DPPG alone (Fig. 5A). This indicates that unlike the DPPC monolayer, a small fraction of the peptide remains in the monolayer even at high surface pressure. Given the strong positive charge of the peptide (+6) it is reasonable to assume that the surface concentration of pEM-2 in DPPG monolayer is larger than in DPPC due to electrostatic attraction.

AFM topography measurements reveal small nanoscale aggregates (Fig. 6) in the pEM-2/DPPG monolayers. At lower peptide concentration (100 nM) these aggregates are 1–4 nm in height and 20–60 nm in diameter and are organized into large micro scale domains. However, unlike pEM-2/DPPC monolayers, the boundaries of these domains are smooth and well defined. At this peptide concentration the liquid expanded–liquid condensed transition is still clearly visible in the LB isotherm (Fig. 5A).

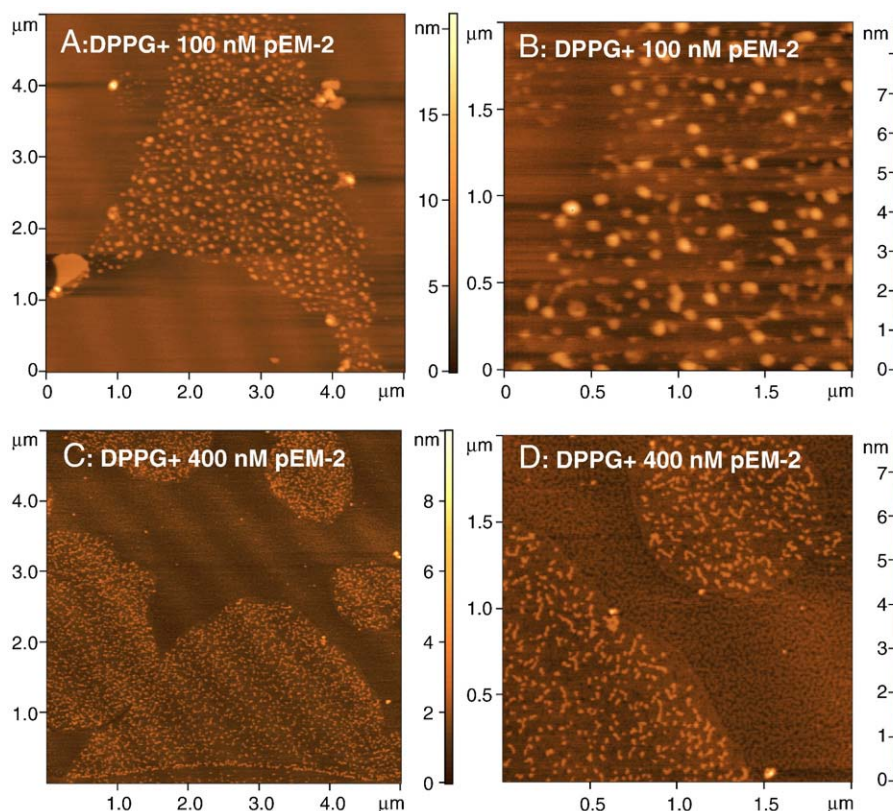


Fig. 6. AFM topography images of DPPG/pEM-2 monolayers at 30 mN/m. pEM-2 subphase concentrations were 100 nM and 400 nM.

At higher peptide concentration (400 nM) above which the plateau corresponding to the phase transition in DPPG monolayer disappears, the topography of the monolayer changes. The size of the small nanoscale aggregates decreases to 1.5–2 nm in height and 10 nm laterally. The micro scale domains become more circular with well defined edges. Finally, there are some small holes 0.5 nm deep observed in the area between the micro scale domains. Similar to DPPC/pEM-2 monolayer the nanoscale aggregates appear most likely as a result of the peptide/lipid interactions and contain molecules of both types. However, unlike DPPC, the nanoscale aggregates in DPPG monolayer are well separated from each other.

Since the presence of the peptide significantly affects the phase behavior of the lipid monolayer it is possible that the large circular domains are in fact areas of DPPG in liquid condensed phase whereas the areas with small holes correspond to the liquid expanded phase. Similar effect of other peptides on the behavior of lipid monolayers has been observed before [22]. The different pattern of peptide distribution as well as higher surface concentration of the peptide in anionic DPPG as compared with zwitterionic DPPC lipid monolayers indicates a different nature of interactions between the peptide and the two phospholipid model cell membranes.

4.5. Calcein leakage assay

Finally, to assess the ability of pEM-2 to rupture bacterial cell membrane, calcein leakage assay was performed (Fig. 7). Five different model cell membranes were used: two single lipid membranes (DPPC and DPPG) and three model mixtures mimicking gram positive (*B. subtilis*, *S. aureus*) and gram negative (*E. coli*) bacteria. The amount of calcein release from the vesicles at different peptide concentrations after approximately 15 min was determined. Results show similar lytic activity of pEM-2 to DPPC, *E. coli*, *B. subtilis*, and *S. aureus* model vesicles. The calcein leakage experiment indicates that the fluorescence signal increases rapidly after the peptide addition and is observed at relatively high peptide to lipid ratios. The fluorescence intensity increases by around 20% for those model cell membranes at the peptide/lipid ratio of 1/10 (Fig. 7). At the same time, effect of the peptide on anionic DPPG vesicles is considerably weaker: only about 5% calcein release was observed at the pEM-2/DPPG ratio of 1/10. This observation is quite different from the monolayer experiments where the peptide showed much higher affinity to anionic DPPG. Therefore it is possible that interactions other than electrostatic play the main role in pEM-2 lytic activity.

Interactions of antimicrobial peptides with bacterial cell membranes represent a multi step process which includes: initial recognition and binding, accompanied by the peptide conformational transformation, peptide aggregation, insertion into the membrane,

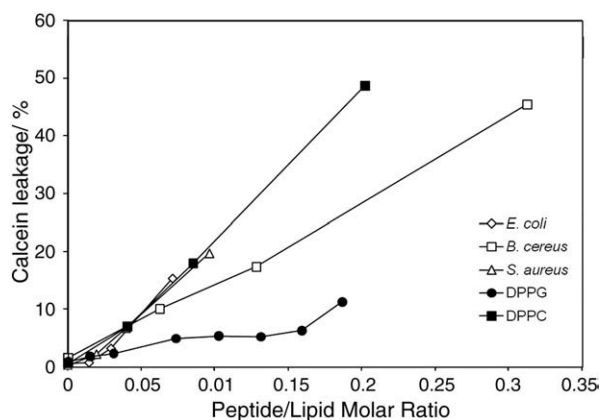


Fig. 7. Calcein fluorescence signal increase measured about 15 min after the addition of pEM-2 into DPPC, DPPG, *E. coli* model, *S. aureus* model and *B. subtilis* model vesicles.

and finally disruption of cell membrane [1–6,30,31]. LB monolayer surface tension measurements allowed us to monitor the initial step of peptide binding. Even though the kinetics of the reaction is limited by peptide diffusion in the trough, the degree of peptide binding to the monolayer depends on the initial peptide/membrane interactions. It is conceivable that for this initial recognition and binding step, the nature of the lipid headgroup rather than other membrane properties (such as thickness and lateral mobility) plays the determining role. Therefore in this context LB measurements represent a fairly good model of this initial step and indicate that electrostatic interactions contribute considerably to this process [25].

On the other hand calcein leakage assay monitors the final step of the AMP/membrane interactions: formation of pores and/or membrane rupture. In the experiment the degree of membrane disruption is estimated from the relative amount of calcein released outside the vesicles. It appears that membrane rupturing ability of pEM-2 does not correlate with the membrane charge, at least for the model membranes used in the present study, suggesting that electrostatic interactions might not play such a critical role in pEM-2's ability to rupture the membrane [13].

Therefore, although the initial recognition and binding of pEM-2 is driven by electrostatic interactions the membrane lytic activity of the peptide is governed by other interactions such as hydrophobic and depends strongly on the bacterial membrane composition and physico chemical properties. This conclusion is supported by the correlation between the number of Trp residues and the bactericidal activity of other derivatives similar to pEM-2 [13]. With increasing number of Trp residues from 1 to 3, bactericidal potency of the peptides was found to increase, suggesting that hydrophobic interactions are critical for membrane damage [13]. This is also consistent with previous studies of other antimicrobial peptides [32]. For example, although the membrane charge was found to play a significant role in the rates of the cell-penetrating peptide transport binding to the cell membrane, dye efflux occurred at about the same rate from charged and uncharged vesicles [30,33].

Recent studies of pEM-2 by UV resonance Raman spectroscopy demonstrated that in a membrane mimicking environment the peptide changes its conformation [34] and likely folds into an α helical amphipathic structure on the membrane surface. Since pEM-2 is a relatively short peptide it is unlikely that the peptide forms permanent pores in the membrane. Besides, calcein leakage is observed at relatively large peptide/lipid ratios. For these reasons, a carpet mechanism or the recently proposed mechanisms based on interfacial activity [31,35] of the peptide are the most likely mechanisms of pEM-2 action in DPPC, *E. coli*, *B. subtilis*, and *S. aureus* models, but not in DPPG. More support for this hypothesis comes from the peptide's ability to induce the formation of nanoscale aggregates in phospholipid monolayers. Lateral organization of these aggregates strongly depends on the membrane composition and is different for DPPC and DPPG models. It is not clear at the moment if similar aggregates occur at the bacterial cell membrane. Further microscopic investigations of pEM-2 interactions with phospholipid bilayers will help to establish these mechanisms in more details.

5. Conclusion

In this work we demonstrated that a short synthetic antimicrobial peptide derived from the C-terminus of myotoxin II from the venom of the snake *Bothrops asper* has greater affinity to anionic monolayer leading to higher peptide surface concentration in anionic rather than in zwitterionic monolayer. At the same time, peptide lytic activity appears to be strongly dependent on the model cell membrane composition. This suggests that although electrostatic interactions play a major role in the initial recognition and membrane binding of the peptide, it is rather the membrane lipid composition and hydrophobic interactions that determine pEM-2 lytic activity.

Acknowledgments

We would like to thank Graham Galway and Stahs Pripotnev for help with the preparation of the manuscript. Financial support was provided by NSERC, CFI and Carleton University.

References

- [1] M.R. Yeaman, N.Y. Yount, Mechanisms of antimicrobial peptide action and resistance, *Pharm. Rev.* 5 (2003) 28–56.
- [2] N. Mookherjee, R.E.W. Hancock, Cationic host defence peptides: innate immune regulatory peptides as a novel approach for treating infections, *Cell. Mol. Life Sci.* 64 (2007) 922–933.
- [3] R.E.W. Hancock, H.-G. Sahl, Antimicrobial and host-defence peptides as novel anti-infective therapeutic strategies, *Nature Biotech.* 24 (2006) 1551–1557.
- [4] K.A. Brogden, Antimicrobial peptides: pore formers or metabolic inhibitors in bacteria? *Nature Rev. Microbiology* 3 (2005) 238–250.
- [5] S.H. Marshall, G. Arenas, Antimicrobial peptides: a natural alternative to chemical antibiotics and a potential for applied biotechnology, *Electr. J. Biotech.* 6 (2003) 1–12.
- [6] M. Zasloff, Antimicrobial peptides of multicellular organisms, *Nature* 415 (2002) 389–395.
- [7] R.E.W. Hancock, M.G. Scott, The role of antimicrobial peptides in animal defences, *Proc. Nat. Acad. Sci.* 97 (2000) 8856–8861.
- [8] J.P.S. Power, R.E.W. Hancock, The relationship between peptide structure and antibacterial activity, *Peptides* 24 (2003) 1681–1691.
- [9] D.A. Devine, R.E.W. Hancock, *Mammalian Host Defense Peptide*, Cambridge University Press, 2004.
- [10] C.R. Mateo, J. Gomez, J. Villalain, J.M. Gonzalez-Ros, *Peptide–Lipid Interactions: New Approaches and Emerging Concepts*, Springer-Verlag Berlin Heidelberg, Germany, 2006.
- [11] N. Chongsiriwatana, J.A. Patch, A.M. Czystewski, M.T. Dohm, A. Iankin, D. Gidalevitz, R.N. Zuckermann, A.E. Barron, Peptoids that mimic the structure, function, and mechanism of helical antimicrobial peptides, *Proc. Nat. Acad. Sci.* 105 (2008) 2794–2799.
- [12] C. Santamaria, S. Larios, S. Quiros, J. Pizazzro-Cerda, J. Gorvel, B. Lomonte, E. Moreno, Bactericidal and antiendotoxic properties of short cationic peptides derived from a snake venom Lys49 phospholipase A₂, *Antimicrob. Agents Chemoth.* 49 (2005) 1340–1345.
- [13] C. Santamaria, S. Larios, Y. Angulo, J. Pizarro-Cerda, J.-P. Gorvel, E. Moreno, B. Lomonte, Antimicrobial activity of myotoxic phospholipases A₂ from crotalid snake venoms and synthetic peptide variants derived from their C-terminal region, *Toxicon* 45 (2005) 807–815.
- [14] L. Páramo, B. Lomonte, J. Pizarro-Cerdá, J.A. Bengoechea, J.P. Gorvel, E. Moreno, Bactericidal activity of Lys49 and Asp49 myotoxic phospholipases A₂ from *Bothrops asper* snake venom-synthetic Lys49 myotoxin II-(115–129)-peptide identifies its bactericidal region, *Eur. J. Biochem.* 253 (1998) 452–461.
- [15] L.A. Murillo, C.-Y. Lan, N.M. Agabian, S. Larios, B. Lomonte, Fungicidal activity of a phospholipase A₂-derived synthetic peptide variant against *Candida albicans*, *Res. Esp. Quimioterap* 20 (2007) 330–333.
- [16] C. Araya, B. Lomonte, Antitumor effects of cationic peptides derived from Lys49 phospholipase A₂ homologues of snake venoms, *Cell. Biol. Int.* 31 (2007) 263–268.
- [17] R.F. Epand, P.B. Savage, R.M. Epand, Bacterial lipid composition and the antimicrobial efficacy of cationic steroid compounds (Ceragenins), *Biochim. Biophys. Acta* 1768 (2007) 2500–2509.
- [18] K.A. Edwards, J.C. March, GM1-functionalized liposomes in a microtiter plate assay for cholera toxin in *Vibrio cholerae* culture samples, *Anal. Biochem.* 368 (2007) 39–48.
- [19] M. Majerowicz, A.J. Waring, S. Wen, F. Bringezu, Interaction of the antimicrobial peptide dicynthaurin with membrane phospholipids at the air–liquid interface, *J. Phys. Chem. B* 111 (2007) 3813–3821.
- [20] G. Signor, S. Mammi, E. Peggion, H. Ringdorf, A. Wagenknecht, Interaction of bombolitin III with phospholipid monolayers and liposomes and effect on the activity of phospholipase A₂, *Biochemistry* 33 (1994) 6659–6670.
- [21] R. Maget-Dana, The monolayer technique: a potent tool for studying the interfacial properties of antimicrobial and membrane-lytic peptides and their interactions with lipid membranes, *Biochim. Biophys. Acta* 1462 (1999) 109–140.
- [22] T. Plenat, S. Deshayes, S. Boichot, P.E. Milhiet, R.B. Cole, F. Heitz, C. Le Grimmellec, Interaction of primary amphipathic cell-penetrating peptides with phospholipid-supported monolayers, *Langmuir* 20 (2004) 9255–9261.
- [23] V. Vie, N. Van Mau, L. Chaloin, E. Lesniewska, C. Le Grimmellec, F. Heitz, Detection of peptide–lipid interactions in mixed monolayers, using isotherms, atomic force microscopy, and Fourier transform infrared analyses, *Biophys. J.* 78 (2000) 846–856.
- [24] K. Wagner, N. Van Mau, S. Boichot, A.V. Kajava, U. Krauss, C. Le Grimmellec, A. Beck-Sickinger, F. Heitz, Interactions of the human calcitonin fragment 9–32 with phospholipids: a monolayer study, *Biophys. J.* 87 (2004) 386–395.
- [25] D. Gidalevitz, Y. Ishitsuka, A.S. Muresan, O. Kononov, A.J. Waring, R.I. Lehrer, K.Y. C. Lee, Interactions of antimicrobial peptide protegrin with biomembranes, *Proc. Natl. Acad. Sci.* 100 (2003) 6302–6307.
- [26] X.-M. Yang, D. Xiao, S.J. Xiao, Yu. Wei, Domain structures of phospholipid monolayer Langmuir–Blodgett films determined by atomic force microscopy, *Applied Phys. A* 59 (1994) 139–143.
- [27] D.Y. Takamoto, M.M. Lipp, A. von Nahmen, K.Y.C. Lee, A.J. Waring, J.A. Zasadzinski, Interaction of lung surfactant proteins with anionic phospholipids, *Biophys. J.* 81 (2001) 153–169.
- [28] L. Dubreil, V. Vié, S. Beaufils, D. Marion, A. Renault, Aggregation of puroindoline in phospholipid monolayers spread at the air–liquid interface, *Biophys. J.* 85 (2003) 2650–2660.
- [29] J. Minones Jr., P. Dynarowicz-Latka, J. Minones, J.M. Rodriguez Patino, E. Iribarnegaray, Orientational changes in dipalmitoyl phosphatidyl glycerol Langmuir monolayers, *J. Colloid Interface Sci.* 265 (2003) 380–385.
- [30] L.E. Yandek, A. Pokorny, A. Floren, K. Knoelke, U. Langel, P.F. Almeida, Mechanism of the cell-penetrating peptide transportan 10 permeation of lipid bilayers, *Biophys. J.* 92 (2007) 2434–2444.
- [31] R. Rathinakumar, W.C. Wimley, Biomolecular engineering by combinatorial design and high-throughput screening: small soluble peptide that permeabilize membranes, *J. Am. Chem. Soc.* 130 (2008) 9849–9858.
- [32] O. Toke, Antimicrobial peptides: new candidates in the fight against bacterial infections, *Biopolymers* 80 (2005) 717–735.
- [33] L.E. Yandek, A. Pokorny, P.F. Almeida, Small changes in the primary structure of transportan 10 alter the thermodynamics of its interactions with phospholipid vesicles, *Biochemistry* 41 (2008) 3051–3060.
- [34] B. Quan, A. Ianoul, UV resonance Raman spectroscopy probes the localization of tryptophan containing antimicrobial peptides in lipid vesicles, *J. Raman Spectroscopy* 40 (2009) 260–263.
- [35] R. Rathinakumar, W.F. Walkenhorst, Broad spectrum antimicrobial peptides by rational combinatorial design and high-throughput screening: the importance of interfacial activity, *J. Am. Chem. Soc.* 131 (2009) 7609–7617.